Astron. Astrophys. 348, 1020–1034 (1999)

ASTRONOMY AND ASTROPHYSICS

Coordinated radio continuum observations of comets Hyakutake and Hale–Bopp from 22 to 860 GHz

W.J. Altenhoff[1], J.H. Bieging[2], B. Butler[3], H.M. Butner[1,4], R. Chini[5], C.G.T. Haslam[1], E. Kreysa[1], R.N. Martin[2,4], R. Mauersberger[2], J. McMullin[3,4,6], D. Muders[1,4], W.L. Peters[2,4], J. Schmidt[1], J.B. Schraml[1], A. Sievers[7], P. Stumpff[1], C. Thum[8], A. von Kap-herr[1], H. Wiesemeyer[8], J.E. Wink[8], and R. Zylka[1,9]

[1] Max-Planck-Institut für Radioastronomie, Auf dem Hügel 69, D-53121 Bonn, Germany, (wja@mpifr-bonn.mpg.de)
[2] Steward Observatory, The University of Arizona, Tucson, AZ 85721, USA
[3] National Radio Astronomy Observatory, P.O. Box 0, Socorro, NM 87801, USA
[4] Sub-Millimeter Telescope Observatory, University of Arizona, Tucson, AZ 85721, USA
[5] Astronomisches Institut der Ruhr-Universität Bochum, Universitätsstrasse 150/NA 7, D-44780 Bochum, Germany
[6] National Radio Astronomy Observatory, P.O. Box 2, Green Bank, WV 24944, USA
[7] Instituto de Radioastronomia Millimetrica (IRAM), Avenida Divina Pastora 7 Nucleo Central, E-18012 Granada, Spain
[8] Institut de Radio Astronomie Millimétrique, F-38406 St. Martin d'Hères, France
[9] Institut für Theoretische Astrophysik (ITA), Universität Heidelberg, Tiergartenstrasse 15, D-69121 Heidelberg, Germany

Received 10 February 1999 / Accepted 28 June 1999

Abstract. We have observed both Comets Hyakutake and Hale–Bopp close to perigee with several telescopes at frequencies between 30 and 860 GHz for an extended period of time. The observed "light" curves can be described as a simple function of heliocentric and geocentric distances without any outburst or noticeable variability with time.

Our most sensitive diameter estimate for C/Hyakutake resulted in an upper limit of 2.1 km. The nuclear diameter of C/Hale–Bopp was determined to 44.2 km after separation from the halo emission.

The central part of both halos can be represented by a Gaussian with a linear size at half power points of 1870 and 11080 km for Hyakutake and Hale–Bopp, respectively. The spectral index for both comets is α = 2.8, indicating a similar particle size distributions in the halo of these comets. For Hale–Bopp the extended emission could be traced to more than 10^5 km from its nucleus.

The derived masses, contained in the halo depend strongly on the assumed physical properties of the halo particles. With κ(1mm) = 75 cm^2/g, possibly more appropriate for comets, a halo mass of $6\ 10^{10}$ g is derived for Hyakutake and of $8\ 10^{12}$ g for Hale–Bopp.

Key words: radiation mechanisms: thermal – comets: general – comets: individual: C/Hyakutake – comets: individual: Hale-Bopp – radio continuum: ISM

1. Introduction

Since the appearance of Comet Arend-Roland (1957 III) it has been tried to detect radio continuum radiation of comets. Hobbs et al. (1975) reported the radio detection of Comet Kohoutek (1973 XII) with the Green Bank interferometer; the strong, transient signal was explained by an icy grain halo model. The signal of Comet IRAS-Araki-Alcock (1983 VII), found by Altenhoff et al. (1983) could be explained by the nuclear emission. The signal of Comet P/Halley, monitored over a longer time in 1985/6 by Altenhoff et al. (1989), showed in addition to the nuclear emission a steady halo contribution. After the Halley campaign a detailed review of cometary radio observations was given by Crovisier & Schloerb (1991). Jewitt & Luu (1992) added a series of submillimeter detections with the JCMT. Most of these cometary observations were done with sensitive bolometers near 300 GHz, giving little spectral information for physical interpretations.

When Comet Hale–Bopp (C/1995 O1) was detected, it seemed highly probable that it would become a bright radio comet near perigee, allowing observations over a wide frequency range. The comet signal was expected to be variable, e.g. by its changing geo- and heliocentric distance, possibly also by some intrinsic variability, or an outburst, or even by an icy grain halo (IGH) event. Therefore it was planned that the observations should be done simultaneously, covering the mm- and submm-range over an extended period of time to derive the structure of the comet.

Fortunately Comet Hyakutake (C/1996 B2) appeared in the set up phase of observations; its close passage to earth promised a strong cometary signal, allowing to check out the combined observing network: the Heinrich-Hertz-Telescope (HHT) of the SMTO[1] between 250 and 870 GHz, the IRAM 30m telescope at 250 GHz, the IRAM Plateau de Bure Interferometer (PdBI)

Send offprint requests to: W.J. Altenhoff

[1] The Submillimeter Telescope Observatory (SMTO) operates the Heinrich-Hertz-Telescope as a joint facility for the University of Arizona and the Max-Planck-Institut für Radioastronomie.

Table 1. Instrumental parameters for observations of Comet Hyakutake in 1996 and Comet Hale–Bopp in 1997.

Telescope	Observing Epoch [year]	Freuqency [GHz]	Primary Beam ["]	Synthesized Beam ["]	Beam Throw ["]	Comments
HHT/SMTO	1996/7	860	13	-	60	1 Chan bolometer
	"	345	26	-	120	"
	"	250	40	-	160	"
PdBI	1996	214	23	∼1.2	-	4C2 configuration
	"	114	42	∼3.0	-	"
	1997	∼220	22	∼1.7	-	5C1 5C2 configuration
	"	∼90	54	∼3.1	-	"
30m tel.	1996/7	250	11	-	41	19 chan. bolometer
NRAO VLA	1996	22.5	120	∼1.12	-	C-configuration
100m tel.	1997	32	26.5	-	118	beam switching

near 90 and 230 GHz, and the VLA of NRAO[2] at 22 GHz. At this time the 100 m telescope of the MPIfR was out of operation for a major repair. The observations ran between March 19 and April 4, 1996.

The performed trial observations were successful, facilitating the proposed coordinated observations of Comet Hale–Bopp from February 1 to April 27, 1997. This time the 100m telescope of MPIfR was part of the network.

Intermediate reports of the observations of Comet Hyakutake have been given by Altenhoff et al. (1996), and for Comet Hale–Bopp by Bieging et al. (1997) and by Wink et al. (1999).

2. Observations

During the observing periods both comets were mainly visible in day time, which usually limits the chance for observation and the quality of the data. This became true for Comet Hyakutake; within 10 simultaneous observing periods between the Heinrich-Hertz-Telescope and Pico Veleta there was only one period with marginal observing conditions at 860 GHz and no period with usable data at 250 GHz and/or 345 GHz at both sites simultaneously. Atmospheric conditions for Comet Hale–Bopp were much better. During this time 3, 7, and 10 usable observations were obtained at 860, 345 and 250 GHz, respectively, resulting in a good spectral index and "light" curve determination. The instrumental parameters for both observing sessions are collected in Table 1.

2.1. IRAM 30m telescope (Pico Veleta)

The MPIfR 19-channel bolometer at 250 GHz was used for multiple scan, ON-OFF, and ON-THE-FLY map observations. These observing techniques have been used e.g. by Altenhoff et al. (1994), the ON-THE-FLY maps were analysed by the NIC program, documented by Broguiere et al. (1996), and MOPSI, written by Zylka (1997). All three methods gave consistent results.

[2] NRAO is operated by Associated Universities, Inc., under contract with the National Science Foundation.

The 19-channel bolometer is a hexagonally close packed, diffraction limited array operating at 0.3 K. A common filter defines a bandpass centered at 250 GHz. In the first period Ceres was used as a calibrator and e.g. 1413+135 as a pointing and reference source; in the second period NGC7027 was the calibrator and BL Lac and 3C345 were the main pointing sources. Multiple scans through the comets at the beginning of each observing period showed that the (main) signal could be well represented by a Gaussian shape and that the measured flux density per beam from scans or ON-OFF together with the measured beam broadening would allow a good estimate for the integrated flux density. The derivation of the beam broadening will be discussed later. The allocated observing time per day was typically only 2 hours; consequently the time for calibration and sky dip measurements was reduced to the bare minnimum.

In the main part of this paper either the measured flux density per beam is used or the integrated intensity, calculated with the beam broadening to describe the observed time variations (light curves) and the spectral energy distribution of both comets; later it will be estimated how good the Gaussian approximation is.

2.2. SMTO Heinrich-Hertz-Telescope (Mt. Graham)

The observations were done with the four colour bolometer, consisting of four diffraction limited bolometers in a common ^{3}He cryostat. The effective frequencies are 250 GHz, 345 GHz, 670 GHz, and 860 GHz. Only one bolometer can be coupled to the telescope at a time, but because all four are operational, change over to a different frequency takes only a few minutes.

We used beam switching, chopping horizontally with the subreflector at a rate of 2 Hz. Since atmospheric transmission is very similar at the 670 GHz and 860 GHz bands, only the latter was used for a better spectral index determination. Some essential instrumental parameters are listed in Table 1. The half power beamwidths Θ_b, reported here for these bolometers, are bigger than expected for the respective frequencies, possibly as a result of under-illumination of the main reflector. The calibration takes this error into account. The only negative consequence is a reduction in sensitivity.

For the cometary observations the ON-OFF technique was used to obtain an optimal signal to noise ratio. It is similar to that used at the 30m telescope. The size correction for the total flux density was derived from the beam broadening by the comet, measured at 250 GHz with the 30m telescope. In the first period the calibration was related to Mars and Uranus, in the second period mainly to K3-50, NGC7538, and W3OH with the scale of Sandell (1994).

2.3. IRAM interferometer (Plateau de Bure)

The Plateau de Bure interferometer was used in configuration 4C2 for Comet Hyakutake and in configuration 5C1 (5C2 last period) for Comet Hale–Bopp. Simultaneously with our observations spectroscopic measurements were done by Dr. Bockelée-Morvan and associates, to whom the choice of frequencies was left for their molecular line search. The effective baselines ranged from $\sim$25 to $\sim$180 m. For these observations 3 units of the correlator were assigned to the 90 GHz and 230 GHz receivers, respectively. One of each was at narrow bandwidth for molecular observations. The other two pairs were used at 160 MHz adjacent to the line frequencies.

The observing cycle for Hale–Bopp was: pointing, focusing, 4 min of crosscorrelation on the phase calibrator, one autocorrelation ON-OFF on the comet, and three 17 to 20 min of crosscorrelation on the comet; the cycle was finished by another autocorrelation ON-OFF on the comet. For Hyakutake the cycle did not contain the autocorrelation ON-OFFs. The telescopes tracked the comet to second order. For this, we provided precise ephemerides and up to second order derivatives as well as geocentric radial velocity each 60 min for Hale–Bopp, each 10 min for Hyakutake. The velocity was kept constant for each of the observations in the cycle at the value at the beginning of this observation.

Calibrator for Comet Hyakutake was 1413+135, and the bandpass was measured on 3C273. Calibrator for Comet Hale–Bopp was BL Lac (2200+420). MWC349 was used to determine the flux density of BL Lac at the frequency used. 250 GHz fluxes were also provided from the 30m telescope and showed no variation during the days concerned, For bandpass calibration 0415+373, 3C273, and NRAO530 were measured.

The evaluation was done with the standard program CLIC (Lucas 1996). The amplitude calibration is based on $S(\nu) = 2.3\,\nu^{-0.30}$ for BL LAC and $S(\nu) = 0.86\,\nu^{-1.00}$ for 1413+135, where ν is in GHz. To produce the uv- tables all lines seen in the ON-OFFs and additionally all lines listed in the line catalog, supplied to us by Bockelée-Morvan, were blanked out. The uv-tables were processed and cleaned with the standard program GRAPHIC/MAPPING (Guilloteau et al. 1997).

2.4. NRAO V.L.A. (Socorro)

The VLA consists of 27 25-m antennas spread out in a Y shape on the plains of San Augustin, New Mexico. It was used to observe Comet Hyakutake at a frequency near 22 GHz (K-band). The VLA electronics system allows 2 independent frequency ranges to be received, which were centered at 22.4351 and 22.8351 GHz. Stokes LL and RR were measured independently then combined into total intensity (Stokes I). The total equivalent bandwidth after combining the 2 Stokes and 2 frequency bands is about 190 MHz.

For the observations, the following observing strategy was employed. Time variable phases and amplitudes were adjusted by monitoring a nearby point source calibrator. Absolute flux densities were tied to a relatively strong point source with presumed known flux density. The absolute calibration scale should be good to about 5-10 %. Every hour, a special pointing observation at X-band (3.5 cm) was done to adjust the pointing of the individual antennas. The opacity and system temperatures were determined by the TIP procedure. Data reduction was performed in the AIPS processing package. After initial data inspection and flagging, calibration solutions for the nearby calibrator were transferred to the comet data, and these data were used to make maps of the sky brightness distribution.

Comet Hyakutake was observed on 1996 March 25 and 29. The VLA was in the C configuration at the time, with physical separation of antennas from about 35 m to about 3.4 km. All 27 antennas were tuned to K-band on both dates. The comet was observed for 3 hours on March 25 and 2 hours on March 29. The nearby calibrators used were 1436+636 on the 25th and 0217+738 on the 29th. The absolute calibrator was 3C286, with assumed flux densities of 2.496 and 2.500 Jy in the two frequency bands. Weather was good during both observing periods with zenith opacities near 5 %, and total system temperatures near 150 K.

2.5. MPIfR 100m telescope (Effelsberg)

The new 32 GHz multibeam system at the secondary focus has three horns with two channels, each with a bandwidth of 2 GHz. The signals of the total power receivers can be used for "software beam switching" to surpress atmospheric noise. This receiver system was still in the commissioning phase during this observation, so the performance was not fully optimized. Of the five scheduled observing periods, three were lost due to adverse weather conditions.

Observations were done with multiple scans across the two near beams; by folding the scan around the center between both beams one can optimize the integration on source and minimize the signal of confusing sources, which the telescope is crossing while following the comet. As another safegard against confusion the path of the comet was compared with the 4.85 GHz sky survey of Gregory & Condon (1991) with a limiting sensitivity of 25 mJy. During observations the comet did not cross any source in the catalog. This double beam observing method has been used successfully by e.g. Altenhoff et al. (1983) for the observation of Comet IRAS-Araki-Alcock. The observed signals were calibrated against NGC7027, using the scale of Ott et al. (1994).

Table 2. Observed Gaussian half power widths Θ_b.

Source	N	Θ_b ["]	σ ["]	Method/Comm.
Point S.	17	11.2	0.1	Scan
Comet	11	16.0	0.2	Scan
BL LAC	1	12.1	-	Map
Comet	10	16.1	0.4	Map
Halo	10	11.5	0.2	de-convolved

2.6. Ephemerides

The ephemerides for the Plateau de Bure Interferometer and the VLA were based on the calculations by P. Rocher (Bdl), and the orbital elements by D.K. Yeomans (JPL). Similarly in the first period the ephemerides at the other sites were based on the most recent orbital elements of Yeomans (solutions 14 to 28) by adjustment of the osculating epoch to the date of observation by taking into account the perturbations of the planets (DE200). In the second period the orbital elements of Marsden (1996, 1997) were used to calculate the ephemerides. For Comet Hyakutake both sets of orbital elements resulted in nearly identical ephemerides, for Comet Hale–Bopp there were small but significant differences between the ephemerides and also between the ephemerides and the observed position of the comet.

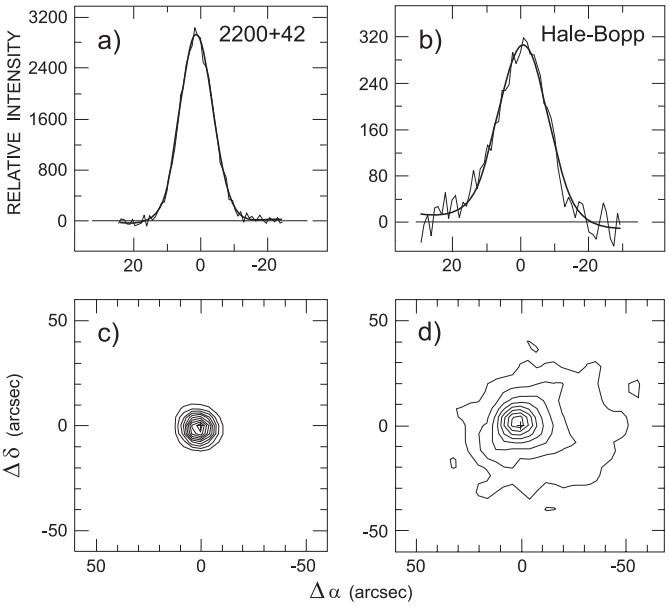

Fig. 1. **a** Scan through BL Lac on Mar. 24, 97 at 250 GHz. Gauss fit: 11.39″. **b** Same scan through Comet Hale–Bopp on March 24, 97. Gaussfit: 17.19″. **c** Map of Bl Lac (point source) on Mar. 19, 97. **d** Average of four bolometer maps of Comet Hale–Bopp between March 13 and 16.

3. Comet Hale–Bopp

Against the sequence of observations we start with Comet Hale–Bopp, because the data reduction technique can be better shown with the more significant signals and the more complete set of data. The first radio observations of Comet Hale–Bopp, on 1997 February 1 by Kreysa et al. (1997) showed that the radio emission was stronger than expected. From the first observation the signal at Pico Veleta was strong enough to measure the position by scans. Fig. 1b shows such a cut through the comet, an average of 32 subscans, which is well represented by a Gaussian fit. For comparison Fig. 1a shows a scan through the point source BL Lac. The obvious beam broadening can be used to determine the halo size, if there is no significant fine structure around the comet. Figs. 1c and 1d show maps around BL Lac and the comet (an average of four maps on consecutive days to reduce the noise). The average cometary emission can be described by a strong compact Gaussian source (halo), superimposed possibly on a weak, very extended structure. The emission by the nucleus, detected by Wink & Bockelée-Morvan (1997) with the PdB interferometer, would hardly be visible as a weak point source on this scale.

3.1. Halo

The halo size at 250 GHz was derived either from Gaussian fits to the Azimuth and Elevations scans or from a two dimensional Gaussian fit in the bolometer maps with the standard evaluation program NIC, giving the major and minor axis of the ellipse at half power. The results are compiled in Table 2. N is the number of observations; the large number of point source observations indicates that on several days both BL Lac and 3C345 were measured. The deconvolution of the comet was done day by day, thus allowing to derive an error limit for the result. BL Lac was mapped only once, giving a high value for the Θ_b, obviously caused by anomalous refraction. The default value of Θ_b, derived for ON-THE-FLY bolometer maps during this period, is 11.0″. The deconvolved source size Θ = 11.5″ can be ascribed to the halo. This halo size will be used to calculate the integrated flux densities from the observed flux densities per beam. At a mean geocentric distance Δ = 1.326 a.u. the deconvolved Gaussian halo size corresponds to a linear diameter of 11080 km.

3.2. Near nuclear activity

The bolometer maps allow the investigation of the near nuclear activity, seen in the optical domaine. But there are two limitations: a.) Sources with moving centres like a comet cannot be reduced by the automated "standard" reduction program NIC, but need special treatment as the comet position needs to be recalculated ideally for each integration point in the map. b.) The time scale of the near nuclear activity may be rather short compared to the observing time needed for a single map.

The first problem can be solved interactively with the evaluation program MOPSI. Three bolometer maps, evaluated this way, are shown in Fig. 2. The first impression is that the extended emission feature is not fully symmetric to the halo, seemingly more extended to the south west. This is also true for the other 7 bolometer maps. The fine structure seen in low contours of

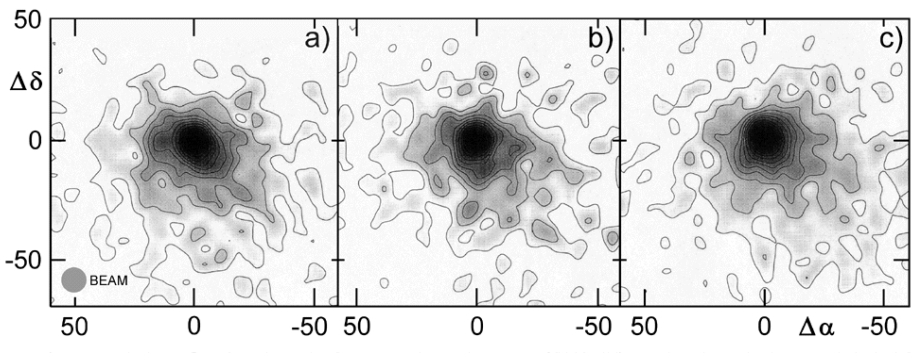

Fig. 2a–c. Bolometer maps of Comet Hale–Bopp at 250 GHz. The lowest contours correspond to 6% of the peak (about 20 mJy/beam), the rms noise is about 15 mJy. Maps are centered on the optimized position of the comet (by pointing). **a** Mar. 13 at UT 09:31, PA(sun) = 164. deg, PA(dust tail) = 313. deg, **b** Mar. 16 at UT 09:53, PA(sun) = 169.5 deg, PA(dust tail) = 317.5 deg, **c** Mar. 24 at UT 08:29, PA(sun) = 180. deg, PA(dust tail) = 329.5 deg. Position angles (PA) of dust tail derived from Kammerer (1997).

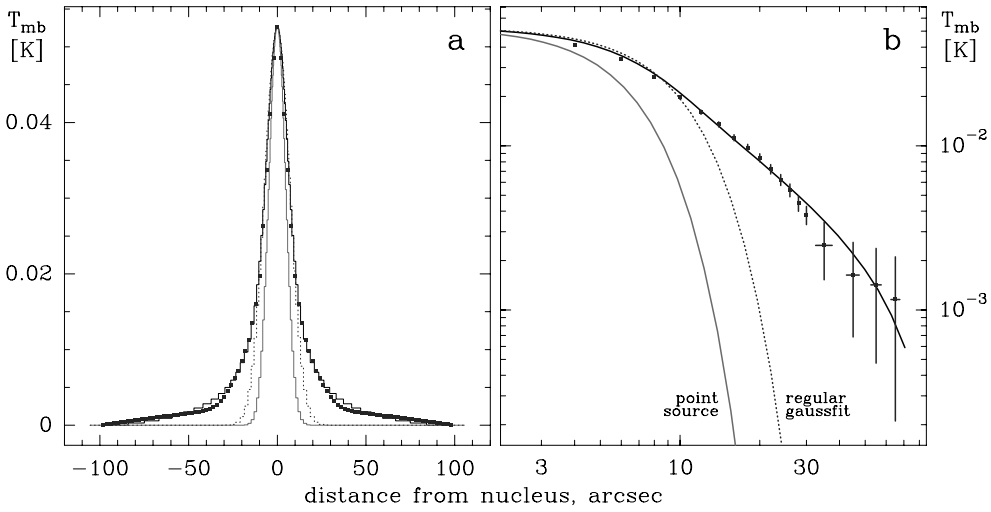

Fig. 3a and b. Cross section through the radio halo of Comet Hale–Bopp at 250 GHz plotted in linear **a** and logarithmic **b** scales. The heavy dots represent the observed mean radial brightness distribution derived from the bolometer maps (Fig. 2) obtained at the 30m telescope. The curves show, from the inside outward, the response to a point source (continuous line), the gaussian fit to the data (dotted), and the model r^{-2} density distribution convolved with the telescope beam.

the extended component seems to be noise, as is suggested by the reduced noise in the averaged map in Fig. 1d. The extended component will be discussed below.

A search for correlation of emission features in the bolometer maps (Fig. 2a-c) with directions to the sun or to the dust tail were negative. Detection of the nuclear jet would not be expected within $\Theta_b \sim 11''$.

For 1997 March 15 and 24 (near observations of Fig. 2b-c) Aguirre (1997) presented IR pictures of multiple expanding dust shells. From these pictures and the rotation period of 11.47 h, derived by Lecacheux et al. (1997), one can derive an arc spacing of about $20''$ and a projected expansion rate of $1.6''$/h for the observing epoch. Such structure would be detectable with the given resolution of $11''$ and a rather short observing time below 1 hour per map. But there is no indication of a shell structure in the radio maps. The missing information on the exact observing time of the IR-maps prevents a more accurate analysis of the correlation of IR and radio data. The short rotation period of the nucleus and the high expansion rate of the arcs do not allow to average maps of different days to search for weak structure near the nucleus.

The observations with the 30m telescope at 250 GHz with its high angular resolution permitted to map the global radial brightness profile of comet Hale–Bopp with an accuracy unprecedented for radio observations of any comet. The mean observed brightness profile of the comet was derived from the bolometer maps in Fig. 2. Pairs of orthogonal cuts through the maps have been extracted and averaged; the result is shown in Fig. 3.

The heavy dots represent the derived brightness distribution. The linear representation (a) shows that the inner part of the particle halo is well represented by a Gaussian fit with the half power width $\Theta_b = 16''$, which is the convolution of the half power beam width of $11.2''$ and the equivalent gaussian half power width of the halo $\Theta_s = 11.5''$. At radii larger than Θ_s, however, the observed emission is clearly stronger than the Gaussian approximation. This figure also shows that the mean emission of the halo extends to $\pm 100''$, corresponding to a nuclear distance of 10^5 km. We have therefore tried to model the radial particle distribution with a r^{-2} profile which falls off at larger radii more slowly than a Gaussian. Such a profile naturally arises if the dust particles lost from the nucleus expand at a constant velocity with a constant size distribution. The resulting $1/r$ brightness distribution was then convolved with a Gaussian beam of $11.2''$. Since the beam switching observations set an instrumental baseline at scan offsets of $\pm 100''$, the r^{-2} model was set to zero at these offsets. This model is shown in the figures as the outer, heavy line; it is a good approximation to the observed mean brightness distribution. The logarithmic representation (b) emphasizes the intermediate range of radii and shows that the surface brightness variation is a power law of the radius, strongly supporting the model used. The given er-

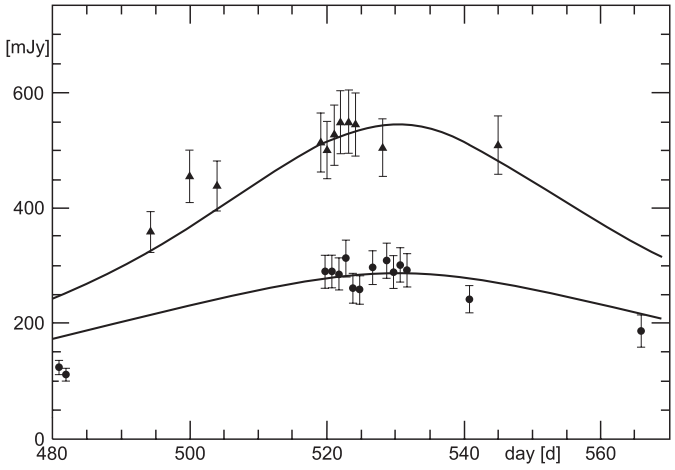

Fig. 4. The observed "light" curves of Comet Hale–Bopp at 250 GHz as function of Julian date. (Julian date = 2450000 + day.) Dots are data of Pico Veleta, triangles data of the Heinrich-Hertz-Telescope. Intensities are normalized to heliocentric distance 0.925 a.u. The plotted curves give the predicted flux densities per beam for the given geocentric distance.

ror limits of the observed surface brightness distribution reflect the uncertainty in the zero level determination; it corresponds to $T_{mb} \sim 0.001$ K.

Naturally, time variation of the dust production rate, and in particular the presence of jets, and possibly instrumental effects like sidelobes and error pattern, may cause departures from a smooth r^{-2} density profile. The instrumental effects seem to be small, because the narrowest error pattern of the 30m telescope near 250 GHz, observed by Garcia-Burillo et al. (1993) has a Gaussian size of 170″, much bigger than the particle halo θ_s; this is supported by pointing scans (e.g. Fig. 1a), which show no indication of significant sidelobes or error pattern. The underestimate of the total flux density by the Gaussian approximation will be discussed later.

3.3. Light curve

The main purpose of the ON-OFF observations was the derivation of the "light curve", i.e., the observed radio signal as function of time. In the simplest case when the constitution of the comet's nucleus and particle halo do not change with time and the cometary radiation is in equilibrium with insolation, the observed flux density only depends on the helio- and geocentric distance, d and Δ respectively; it is proportional to $d^{-0.5}$ and to Δ^{-2}, modified by the partial resolution. This is the same model as used e.g. by Altenhoff et al. (1994) to determine asteroidal sizes from flux densities near 250 GHz. Since the respective distances are known, this prediction for the light curve can be tested with observations.

The observed intensities at 250 GHz are plotted in Fig. 4 as a function of Julian date. Dots stand for values of Pico Veleta, triangles for data of the Heinrich-Hertz-Telescope. Both sets are normalized to the heliocentric distance of d = 0.925 a.u. The observed flux densities per beam from both telescopes have been integrated to (total) flux densities, normalized to Δ = 1.315 a.u. Aside from a small calibration scale error between the two telescopes the average normalized flux density of the comet at 250 GHz is S_ν = 590 mJy. This average is the constant flux density of our model; the predicted flux densities per beam for both telescopes are calculated from this flux density, considering the changing geocentric distance and the partial resolution. The predicted values are shown as solid lines in Fig. 4. They seem to be a reasonable fit to the observations, consistent with this simple cometary model. The scatter relative to the predicted curves during the main period of coordinated observations may be random noise, rather than an indication of variability. This is supported by the fact that the small deviations of both sets of observations are not correlated with each other. Our observing accuracy of 10 % is clearly an upper limit to the variability of the cometary radio emission. This raises some questions about the relation of the rather constant thermal emission and the possibly variable molecular production rates. Additionally, there is no evidence of any transient icy grain halo (IGH) event, as described e.g. by Hobbs et al. (1975) in our or any other published data of this comet. The possibly systematic deviations in the light curve at both ends of the observing time interval will be discussed later.

3.4. The nucleus

The observations on Plateau de Bure resulted in the first interferometric detection of continuum emission of any comet by Wink & Bockelée-Morvan (1997). It is dominated by its nuclear emission. Fig. 5 shows the cleaned maps for four different days of simultaneous observations near 90 and 218 GHz. The circumstances of these observations (date, time, frequency, geo- and heliocentric cometary distance) are listed in Table 3 and also the intensity of a point source, fitted to the data. Assuming that the nuclear brightness temperature is near the equilibrium temperature with solar insolation, the diameter of the nucleus can be calculated from the flux density of the point source, using the Planck formula. The derived values for equilibrium temperature and nuclear diameter D_n are included in Table 3. The interpretation of this diameter depends on the structure of the halo. If e.g. the halo is spherical, the point source fit would fully represent the nucleus, but if the halo can be represented by a r^{-2} distribution, it has a broad variety of spatial frequencies, and the observed diameter is an upper limit to the real nucleus. Considering only the data in the higher frequency band because of the higher angular resolution the average nuclear diameter from the point source fits becomes formally D_n = 57.1 km.

The visibility plots for the observations of March 13, 1997 at 90 and 218 GHz are shown in Fig. 6 to analyse the source structure. To obtain these points, the uv-data were phase shifted on the nucleus, and vector averages of amplitudes were performed in circles of 300 wavelengths width. A series of models were calculated with the density structure found in connection with the extended structure in Fig. 3 and with various nuclear diameters; the visibility of these models was calculated and compared with the visibility plots for all 4 pairs of observations. The

Table 3. Comet Hale–Bopp with Plateau de Bure Interferometer

UT(mean)		ν [GHz]	S_{point} [mJy]	σ [mJy]	Δ [a.u.]	d [a.u.]	T_{eq} [K]	D_n [km]
Mar. 09	12:00	88.63	4.3	0.4	1.3824	0.9991	275.0	60.0
		224.18	23.	2.3	”	”	”	55.1
Mar. 11	10:00	115.21	8.5	1.1	1.3645	0.9860	276.8	63.9
		229.14	31.0	1.6	”	”	”	61.6
Mar. 13	11:00	90.66	6.8	0.4	1.3483	0.9731	278.7	71.5
		218.33	28.1	1.1	”	”	”	60.6
Mar. 16	12:00	90.66	5.0	0.5	1.3299	0.9560	281.2	60.2
		224.18	19.	1.9	”	”	”	51.3

Table 4. Observed positions of Comet Hale–Bopp

UT Date 1997		α_{app} geocentric [s]	δ_{app} [”]	$\Delta\alpha$ [”]	$\Delta\delta$ [”]	α_{2000} topocentric [s]	δ_{2000} [”]
Mar	09.20833	22 14 36.434	39 21 48.62	0.79	5.11	22 14 45.26	39 22 40.8
	09.33333	15 32.250	27 01.33	0.96	5.11	15 40.94	27 55.5
	09.41667	16 09.588	30 29.20	0.80	4.99	16 18.11	31 24.2
	09.50000	16 47.011	33 56.46	1.00	5.11	16 55.33	34 51.5
Mar	11.25000	22 30 18.145	40 44 25.62	1.13	5.02	22 30 27.10	40 45 20.3
		30 18.155	44 25.84	1.24	5.25	30 27.11	45 20.5
Mar	13.33333	22 47 25.365	42 02 02.83	1.38	5.07	22 47 34.40	42 03 55.4
	13.62500	49 54.426	12 16.13	1.40	5.12	50 02.84	13 13.2
Mar	16.66666	23 17 01.299	43 47 27.88	1.84	5.04	23 17 09.99	43 48 26.1
		17 01.300	47 27.92	1.85	5.08	17 09.99	48 26.2

model with the nuclear diameter of 44.2 km gave the best fit to all visibility plots; the solid line in Fig. 6 represents this model. The visibilities at 218 GHz at the longer uv-spacings, which are not sampled at 90 GHz, are scaled to the 90 GHz plot; they fit perfectly into this visibility plot, demonstrating the consistency of the model. Thus we can take the extended structure in the bolometer maps and the partial resolution of the interferometer observations as strong indications for the $1/r$ brightness distribution of the halo. The average diameter of the nucleus, derived from all the visibility plots, is accurate to at least 5 %, with a value

$$D_n = 44.2 \pm 2.3\,\mathrm{km}.$$

3.5. Position offsets from ephemerides

In the interferometer maps in Fig. 5 the expected cometary positions, derived with Yeoman's solution 55, are marked by crosses. The observed radio positions deviate systematically. The observed positions and the deviation from the ephemerides are listed in Table 4. These deviations exceed the expected error limits, quoted by Yeomans. A comparison with ephemerides derived from Yeoman's orbital solution 58 (including optical data near perigee) still confirm the systematic deviations. To test the observing technique asteroid Ceres was observed the same way as the comet; it showed no position error. De Pater et al. (1998) found a similar discrepancy between ephemerides and radio positions for their observing epochs. Also the bolometer observations on Pico Veleta showed a similar position offset. Obviously the nuclear and halo positions coincide. Additionally it should be noted that several molecular line observations show their peak at the observed continuum positions. This discrepancy of all measured radio positions to the optical positions is not yet understood.

Table 5. Integrated flux densities S_ν and photometric diameter, $2R_{ph}$, for Comet Hale–Bopp, normalized to Δ = 1.315 a.u. and d = 0.925 a.u. (24 march 1997).

Telescope	ν [GHz]	S_ν [mJy]	σ [mJy]	$2\,R_{ph}$ [km]
HHT	860	17260.	2590.	375
HHT	345	1305.	130.	251
HHT	250	530.0	53.0	221
IRAM 30m Tel.	250	590.6	59.0	233
MPIfR 100m Tel.	32	1.84	0.4	101

3.6. Spectral energy distribution

The flux densities at 250 GHz, derived from the Gaussian fits and normalized to the epoch of 1997 March 24, were reported above. The corresponding values for the other frequencies were reduced similarly, and all data are compiled in Table 5.

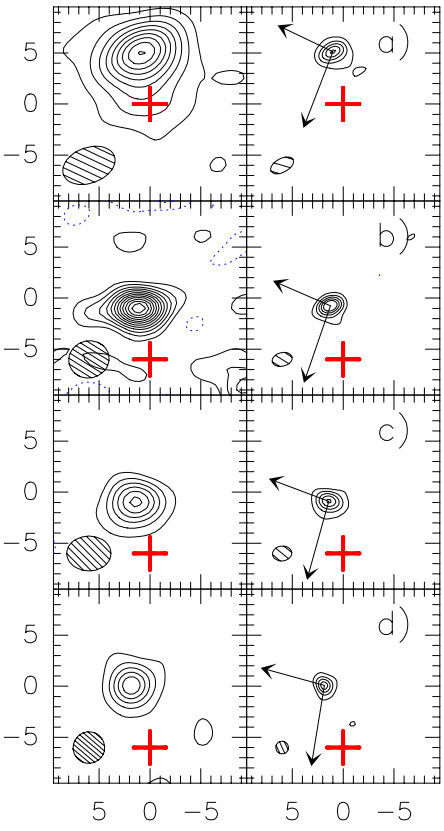

Fig. 5a–d. Cleaned maps of Comet Hale–Bopp, obtained with the PdBI, near 90 GHz (left) and near 220 GHz (right). Arrows indicate directions to the sun and of proper motion. Contour level spacings are 1 mJy for 90 GHz and 5 mJy for 220 GHz. Crosses indicate ephemerides from Yeoman's solution # 55 for the epochs: **a** Mar. 9 (left) UT 05:00, (right) UT 08:00, **b** Mar. 11 (left) UT 14:00, (right) UT 06:00, **c** Mar. 13 (left) UT 15:00, (right) UT 08:00, **d** Mar. 16 (left) UT 16:00, (right) UT 16:00. The corresponding ephemerides are listed in Table 4. Offset positions are in arcsec.

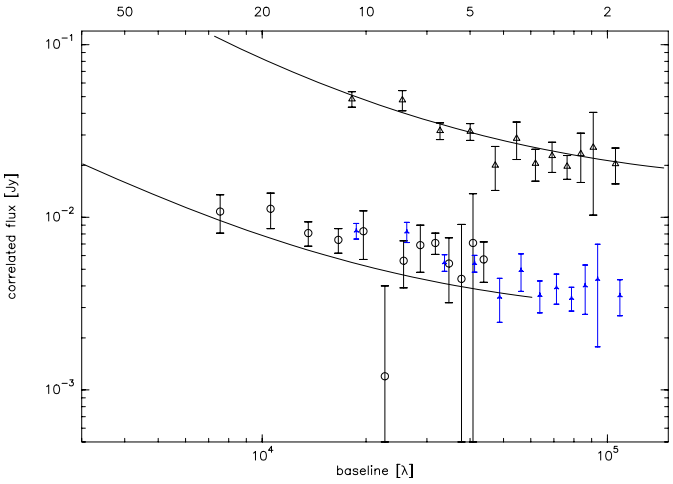

Fig. 6. Correlated amplitudes as function of effective baselines for March 13, 1997 at 218 GHz (triangles) and at 90.7 GHz (circles). Small filled triangles are data of 218 GHz, transformed to 90.7 GHz under assumption of thermal emission. The curves indicate a model with an exponential density distribution as in Fig. 3 together with a thermal point source of 15 mJy at 218 GHz. Above the figure the angular resolution corresponding to the effective baseline is given in arcsec.

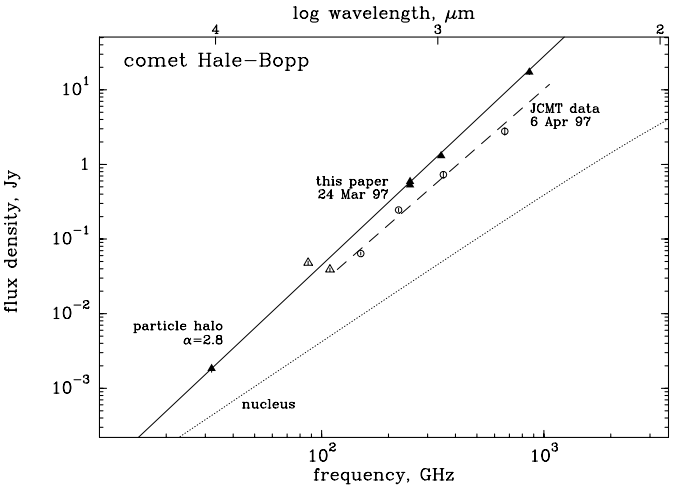

Fig. 7. Spectral energy distribution (SED) of Comet Hale–Bopp. The continuous line fits the data (filled triangles) presented in this paper (Table 5). The dashed line shows the observations of the JCMT, scaled to an aperture of 15.3 arcsec (open circles; Jewitt & Matthews 1999). Measurements near 90 GHz (un-filled triangles) are from de Pater et al. (1998). The dotted line is an estimate of the nuclear emission.

The comet is clearly detected at all frequencies. The quoted error is either the internal error or the uncertainty of the absolute calibration, whichever is higher. All flux densities include a correction for the halo size and therefore represent total flux densities for a Gaussian–shaped source. This is a good representation for the inner halo, as seen in Fig. 1. At larger radii, weak excess emission above a Gaussian shape, coming from the $1/r$ brightness distribution in the halo, becomes significant as shown before. Its exact amplitude and frequency dependence is not known, however, so it is omitted here.

We also give in Table 5 the photometric diameter, $2R_{ph}$, for each observation. R_{ph} is the radius of a circular black body at the temperature of the comet which emits the observed flux density. (The temperature is taken as the equilibrium value, discussed in Sect. 5.1 below.) At all frequencies the photometric diameters are both significantly larger than the size of the nucleus and also much smaller than the observed extent of the halo. The observed flux densities are therefore always dominated by emission from the particle halo. We may also conclude that the halo emission is optically thin at all radio frequencies.

The spectral energy distribution (SED) of the particle halo is seen in Fig. 7 to follow a power law with high accuracy over the whole frequency range from 32 to 860 GHz. The slope α of the power law, $S_\nu \sim \nu^\alpha$, is 2.8 ± 0.1.

For comparison the SED, measured at the JCMT by Jewitt & Mathews (1999), is shown. The results are scaled to an aperture of $15.3''$ with a spectral index of $\alpha = 2.60 \pm 0.13$, in good agreement with our data. Since epochs are different and there are no overlapping size determinations, a calculation of the total flux densities was not attempted.

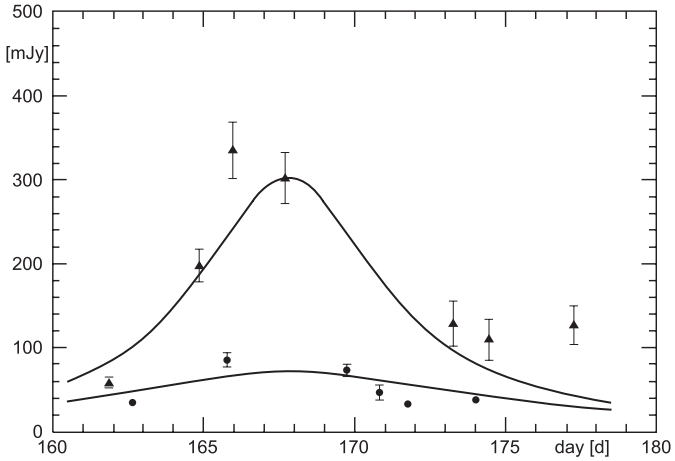

Fig. 8. The "light" curves for Comet Hyakutake at 250 GHz as function of Julian date. (Julian date = 2450000 + day.) Dots are data of Pico Veleta, triangles data of the Heinrich-Hertz-Telescope. Intensities are normalized to heliocentric distance 1.02 a.u.. The plotted curves give the predicted flux densities per beam for the given geocentric distance.

The photometric diameter allows an order of magnitude estimate for the mass in the particle halo. Assuming the thickness of the photometric disk at 250 GHz is one wavelength and the particle density is $1\,\mathrm{g\,cm^{-3}}$, the resulting mass of the halo of Comet Hale–Bopp is $\sim 5\ 10^{13}$ g. A detailed model for the halo particle emission for Comet Hale–Bopp will be presented in Sect. 5.

4. Comet Hyakutake

The adverse weather during the scheduled observations was mentioned above. The close approach of the comet resulted in further problems: the cometary emission near perigee was partially resolved at all frequencies, making size corrections for the total flux density difficult and also uncertain.

4.1. Halo size

The first scans through Comet Hyakutake showed a symmetric Gaussian shape, which was obviously broadened in comparison to a point source. But only the first two observations, when the comet was further away, were sensitive enough for a size determination. An ON-THE-FLY map on the second day marginally showed the comet, but it did not allow an accurate size determination. As additional input the excellent map at 375 GHz, taken by Jewitt & Mathews (1997) with the JCMT near perigee of the Comet, was used. From both sets of data a deconvolved Gaussian half power width of 23″ was derived for the geocentric distance Δ = 0.112 a.u., corresponding to a linear (Gaussian) diameter of 1870 km.

4.2. Light curve

Also for Comet Hyakutake the ON-OFF measurements were used to derive the light curve at 250 GHz. In Fig. 8 the observed flux densities per beam of the 30m telescope are shown as dots, the values of the HHT as triangles. Assuming again that the cometary signals are predictable by the helio- and geocentric distances, the observed flux densities per beam are reduced to total flux densities, normalized to d = 1.02 a.u. and Δ = 0.102 a.u. The resulting average flux density at 250 GHz becomes S_ν = 496 mJy. This value was used to calculate the predicted flux densities per beam for both sites, similarly as for Comet Hale–Bopp; they are shown as solid lines in Fig. 8. The curves predict the general shape of the light curve and the ratio of the observed flux densities per beam for both telescopes reasonably well, the systematic deviations from the predictions at both ends of the time interval will be explained later. The deviations of the observed flux densities per beam from the predictions is attributed to unstable observing conditions, insufficient calibration, and some uncertainty of instrumental parameters (like Θ_b) rather then to intrinsic variability of the comet. Contrary to our light curve Jewitt & Mathews (1997) claim a constant emission of the comet, because their observations on two consecutive days near perigee did not show a "substantial change of the observed flux density"; this is no surprise, because the geocentric distance between their observations changed only by about 10 %!

4.3. Nucleus

All our interferometric observations of the nucleus of Comet Hyakutake are listed in Table 6; they resulted only in upper limits to the size of the nucleus which are all consistent with the first estimate by Harmon et al. (1996), derived by radar observations. The low limit for March 24 is favored by the small geocentric distance. Attempts to detect the nucleus by properly combining either the two simultaneous maps at different frequencies or two maps at different days were not successful; the effective gain of sensitivity by these manipulations may be partially offset by systematic effects.

4.4. Spectral energy distribution

The averaged total flux densities, normalized for March 25, 1996 to Δ = 0.102 a.u. and d = 1.02 a.u. as the 250 GHz data above, are collected in Table 7. The quality of our data is, as noted above, quite poor. In addition to atmospheric problems the instrumental parameters were not known accurately enough to allow an accurate size correction by about one order of magnitude. Such problems are avoided at the JCMT by limiting the angular resolution at any frequency to about 18″, allowing good spectral index determinations. Furthermore, the comet observations by Jewitt & Matthews (1997) are of high quality. By combination of our total flux density measurements at 250 GHz with their spectral index determination, improved physical parameters of Comet Hyakutake can be obtained.

In Fig. 9 the SED of Comet Hyakutake is plotted as a continuous line fitted to our data (filled squares). The dashed line refers to the data of Jewitt & Matthews (1997) (small triangles) with a spectral index α = 2.8. After conversion to flux densities (by size correction) the JCMT data (big triangles) agree well

Table 6. Size estimates for Comet Hyakutake

Instrument	Date	UT(mean) [h]	ν [GHz]	S_{upper} [mJy]	Δ [a.u.]	d [a.u.]	T_{eq} [K]	D_n [km]
PdB Interf.	Mar. 23	01:00	88.6	1.5	0.1257	1.0886	263.5	<3.3
	Mar. 24	01:30	115.1	10.0	0.1096	1.0678	266.0	<5.7
		01:30	241.3	6.0	0.1096	1.0678	266.0	<2.1
	Mar. 29	21:15	88.6	1.5	0.1824	0.9429	283.1	<4.6
		21:15	230.5	8.0	0.1824	0.9429	283.1	<4.1
V.L.A.	Mar. 25	11:00	22.5	0.250	0.1019	1.0386	269.7	<4.2
	Mar. 29	06:00	22.5	0.383	0.1660	0.9571	281.0	<8.4

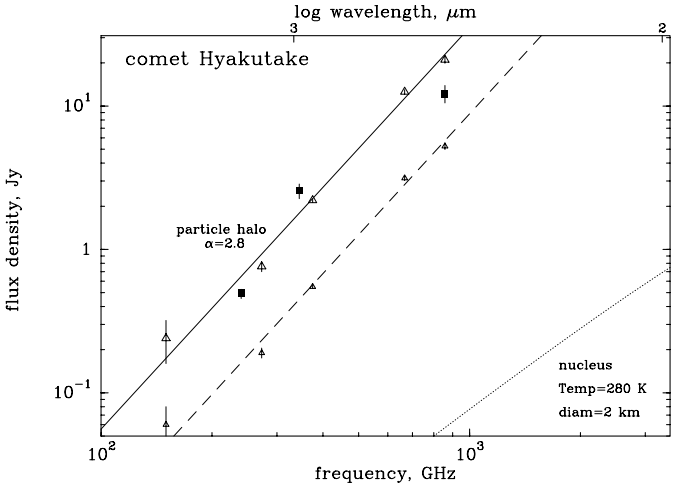

Fig. 9. The SED for Comet Hyakutake, triangles come from Jewitt & Matthews (1997) squares from this paper; the broken line is a fit to flux densities per JCMT beam of ∼18 arcsec, the full line is a fit to flux densities in the Gaussian component. The lower thin line is an estimate of the nuclar emission.

Table 7. Integrated flux densities, normalized to Δ = 0.102 a.u. and d = 1.02 a.u. for Comet Hyakutake

Telescope	ν [GHz]	S_ν [mJy]	σ [mJy]	$2\,R_{ph}$ [km]
HHT	860.	12120.	3400.	25.2
HHT	345.	2560.	600.	29.1
HHT	250.	491.	72.	16.8
IRAM 30m Tel.	250.	500.	50.	17.1

with our SED. Also here the photometric diameter is used to get an order of magnitude estimate of the mass in the halo. At 250 GHz the photometric diameter is 11.6 km, yielding a rough mass estimate of $\sim$2.8 10^{11} g.

5. General discussion

5.1. Equilibrium temperature

For the photometric size determination of the nuclear diameters and for the normalisation in the light curves the same model was used, which Altenhoff et al. (1994) had successfully applied to asteroids. This method assumes a radio emissivity of unity and the comet in temperature equilibrium with insolation. For many comets this equilibrium may not be reached, because e.g. evaporating water ice keeps the surface near 195 K (see e.g. the comet model of Fanale & Salvail 1984).

Considering the size of the observed halos and the evaporation time scale most dust particles must be refractory grains and at least the bigger ones should adjust to the equilibrium temperature; this assumption is possibly supported by the observed heliocentric distance dependence of the halo, which will be discussed below. Even if the nuclear temperature would not vary, the results of the light curves are hardly affected.

De Pater at al. (1985, 1998) have discussed the effective nuclear brightness temperature with frequency as function of surface material, emissivity and depth structure, offering a brightness temperature range from 195 K to 280 K at d $\sim$ 1 a.u.; for their interpretation they adopt 195 K, the sublimation point of water ice, independent of the heliocentric distance.

The very low optical albedo for cometary nuclei (e.g. Halley, Hale–Bopp) of about 3 % indicates that the nucleus is covered by dark material rather than by pure ice. Since the surface depth involved in absorption and emission is of the same order as the wavelength, it seems probable that for mm wavelength (300 GHz) the surface temperature is close to the expected equilibrium temperature. This temperature is supported by far IR observations of the "bare" nucleus of Comet IRAS-Araki-Alcock by Hanner et al. (1985) and of the nucleus of Comet Halley from spacecraft, as reviewed by Yeomans (1991), showing a temperature at least 100 K warmer than expected from a sublimating, icy nucleus. (A more extended observing run on PdBI, sampling a wider heliocentric distance range, could have tested these temperature assumptions for Comet Hale–Bopp, too.) For the discussion here we assume that the effective brightness temperature equals the equilibrium temperature to scale the cometary halo intensities and to calculate the nuclear sizes.

5.2. Model of the halo

SEDs of power–law shape have been found previously for Comet Hyakutake by Jewitt & Matthews (1997) and Altenhoff et al. (1996) and for comet Hale–Bopp by de Pater et al. (1998), Bieging et al. (1997), Jewitt & Matthews (1999); power-law

Table 8. Particle halo model parameters

Parameter		Best Fit	Range	Remark
Particle size distribution:				
minimum radius	a_{min}	1 μm		ill determined
maximum radius	a_{max}	1 cm		
number of particles	n_0			
size distribution index	β	3.9	± 0.1	
Absorption coefficient:				
slope	δ	-1.5	± 0.5	
turn over wavelength	a_c	$2\pi a$	$a_c/2$	not critical
Temperature:				
Hale–Bopp	T_p	285 K		fixed
Hyakutake	T_p	270 K		fixed
Mass:				
Hale–Bopp	M_p	$8 \cdot 10^{12}$ g	factor ~ 2	
Hyakutake	M_p	$6 \cdot 10^{10}$ g	factor ~ 2	

SEDs are well known from observations of interstellar dust, where they are thought to originate from a power–law size distribution, $n(a)da \sim a^{\beta}$, of dust grains with radii a and $\beta = -3.5$ (Mathis et al. 1977; Krügel & Siebenmorgen 1994). In the particle halo model described below we follow this prescription of a power–law distribution of grain radii, characterized by β and a normalization constant n_0. We first estimate the particle mass contained in the total halo by model fitting the observed SED. The radial distribution of the halo emission, its Gaussian width and the excess above a Gaussian at larger radii, will be modelled in a second step.

In estimating the mass of the particle halo from the observed SED, we need to adopt a wavelength dependent absorption coefficient for the different particle sizes which contribute to the mm/submm emission. Rather than assuming specific optical constants for the cometary grains (Walmsley 1985, Jewitt & Matthews 1997), we adopt the less specific but physically plausible concept that the grain absorption efficiency Q_{abs}, defined as the ratio of the absorption cross section C_{abs} to the geometric cross section, is unity for grains larger than a_c and varies as λ^{δ} for $\lambda < a_c$. For a homogenous, non–porous, spherical dielectric particle $a_c = 2\pi a$ and $\delta = -1$ (see e.g. Krishna–Swamy 1986). The cometary particles may have properties departing from these idealizations, and we have therefore kept a_c and δ as free parameters. In maintaining this simplified concept for Q_{abs} we effectively assume that any resonances occuring in the mm/submm wavelength range are smoothed out to a large degree. Calculations of Q_{abs} were made using Mie theory for optical constants of various core/mantle grains. The program (E. Krügel, private communication) gave results in agreement with our simplified concept, while significant departures occured only in some cases at $\lambda \gg 2\pi a$ where they are without relevance to our model.

The list of model parameters in Table 8 further includes the temperature T_p of the particles and their minimum and maximum radii. We assumed that the particles are weakly reflective (optical albedo 0.03) and are in equilibrium with the solar radiation field. The range of particle radii was divided into logarithmic intervals and the emission spectrum from each interval was integrated numerically. The model parameters n_0, β, a_c, and δ were varied until the observed SED was reproduced. The resulting mass of the particle halo, M_p, is relatively insensitive to the values of the model parameters. The allowed ranges are listed in Table 8, from which we conclude that, within a factor 2, the model-derived mass $M_p = 8\ 10^{12}$ g for Comet Hale–Bopp.

The mass of the particle halo for Comet Hyakutake was derived in the same way. Since the spectral indices of the SED are the same for both comets (α = 2.8), their model particle size distributions must also be identical. Using the equilibrium temperature of 270 K for the comet at the position and time of our observations, even though the smallest halo particles may not quite behave as grey bodies, this model yields, within a factor 2, $M_p = 6\ 10^{10}$ g.

5.3. Limitation of the flux density determination

The "integrated" cometary flux densities were derived from ON-OFF measurements, corrected for the apparent size of the halo at the observation. This size information was derived from Gaussian fits to the halo emission. The contribution of the extended structure, not included in the Gaussian fit, is significant. A first estimate was done by measuring planimetrically the difference, giving a contribution of roughly 30 %) to the total flux density. But this difference is dependent on both the integration limits and the accuracy of the long restored scans and is therefore not very precise. Fortunately the first observations with SCUBA by Matthews et al. (1997) allow an independent estimate. They report a total flux density of 2.18 Jy at 353 GHz within the synthetic aperture of 60″. Scaled with spectral index α = 2.8, the total flux at 250 GHz is 830 mJy, about 40 % higher than given above for Gaussian fits. This value should be a good estimate for the contribution of the very extended structure at 250 GHz, and it may be a valid estimate for the other frequencies, too.

5.4. Dust production rate

The dust production rate Q of the comet can be estimated if we assume that the dust particles form a spherically symmetric halo around the nucleus and drift away from it at a constant velocity v_{exp}. The average dust particle therefore resides a time $t_R = R_H/v_{exp}$ inside the observed halo radius R_H, and must be replaced after one residence time t_R. The dust production rate is then simply the mass of the particle halo M_p as derived above, divided by t_R.

While the observed $1/r$ emission profile in Fig. 3 clearly supports the spherical constant velocity outflow model, the value of v_{exp} is observationally not well constrained. Hydrodynamical models of particle entrainment in the gas stream from the nucleus usually give particle velocities dependent on their radius roughly like $a^{-0.5}$ (Crifo 1987). The micron–sized (and smaller) particles attain the maximum velocity, the expansion velocity of the gas observed to be $\sim 1.3\,\mathrm{km\,s^{-1}}$ by Biver et al. (1997). Lisse et al. (1999) report a particle expansion velocity

of 0.4 km s^{-1}, projected on the plane of the sky. Their results, derived from direct mid-IR images of the motions of features in the coma near perigee, probably refers to smaller particles than those that dominate the mm/submm emission. The particles dominating the 250 GHz signal are however much larger and should therefore have lower velocities. For a particle radius of $a = 200\,\mu$m, probably the smallest size contributing efficiently, the model gives ~ 200 m s^{-1}. The largest contributing particle would have a radius of ~ 1 cm and a velocity of 20 m s^{-1}, just large enough to escape from the gravity of the nucleus. An estimate of the particle expansion velocity obtained by taking the geometric mean of the latter two values gives $v_{exp} = 60$ m s^{-1}. The average particle residence time in the halo would then be ~ 26 hours, and the dust production rate $Q = 8\,10^7$ g s^{-1}.

Biver et al. (1997) deduced a gas production rate near perihelion of $\sim 1.4\,10^8$ g s^{-1} (including both water and CO), which, combined with our estimates of the dust rate, implies a ratio of dust/gas production of ~ 0.6.

For Comet Hyakutake the dust production rate, Q, is also derived from an estimate of the average residence time t_R of a dust particle inside the $23''$ halo (equivalent radius 1000 km). Assuming as for Hale–Bopp an expansion velocity of 60 m s^{-1} for the most massive dust particles we obtain $t_R \sim 5$ hours and a dust production rate Q of about $4\,10^6$ g s^{-1}.

5.5. Particle size distribution

We derive a best fit index $\beta = 3.9 \pm 0.1$, not too different from its presumed interstellar value of 3.5. This latter value is believed to characterize a size distribution which derives from collisional fragmentation (Hellyer 1970). Does this mechanism also work in comets? We can show, based on our particle halo model, that the mean free path of the smaller particles is only of the order of 1 km, within 50 km from the nucleus. Collisions among dust particles should therefore be frequent.

5.6. Nature of dust particles

We detect dust out to distances of $100''$, i.e. ~ 70000 km from the nucleus. If these were ice particles whose lifetime is believed not to exceed one day, the particles must have moved at speeds of ~ 1 km s^{-1}. This is close to or even exceeds the gas expansion velocity. According to hydrodynamical models (Crifo 1987) such high speeds may only be reached by the smallest particles whose radii are smaller than a few microns. If particles lose some fraction of their kinetic energy in a near nucleus collision zone, their initial velocities must have been even higher, i.e. their radii even smaller, in order to reach the 70000 km evaporation radius in a few days. Yet our best fit size distribution implies the presence of a substantial mass component with sizes 10 μm up to ≥ 1 mm. It is therefore plausible that the particles dominating the mm/submm light are in fact refractory. Our modelling of the radial brightness distribution gives a near–perfect fit assuming that the size distribution of particles is constant throughout the halo. Our modelling is therefore fully compatible with refractory grains whose size distribution does not change when they flow away from the nucleus.

5.7. Precision of mass estimates

In Table 8 we estimated the error of the halo masses as about a factor of 2 for both comets. This error reflects only the uncertainty in the observations and in the fitting procedure. The error resulting from our poor knowledge of the dust properties is more difficult to assess. A useful recent compilation of models of the dust absorption cross section at submm/mm wavelengths is given in Fig. 15 of Menshchikov & Henning (1996). While there appears to be little scatter between the various models at wavelengths up to 30 μm, the spread between models increases toward the submm, and reaches about a factor 30 near $\lambda = 1$ mm. The lowest value[3], κ(1 mm) = 0.4 cm^2 g^{-1} (per gram of dust), applies to normal interstellar dust (Draine & Lee 1984; Pollack et al. 1994).

In their theoretical study of dust in protostellar cores and circumstellar disks Krügel & Siebenmorgen (1994) came to a similar range of κ(1 mm). Their analysis shows quantitatively how grain growth coupled with the deposition of ice mantles onto porous refractory cores can increase $\kappa(1mm)$ by up to two orders of magnitude above its interstellar value. Our grain model, though very rudimentary in comparison, successfully reproduces their $\kappa(\lambda)$ for those grain size distributions which are dominated by mm sized particles. Such particles are sufficiently large and heterogenous that any resonances due to specific grain materials are smeared out. In particular, we reproduce within 30 percent their model labelled β Pic which characterizes the peculiar dust in the circumstellar disk of β Pic. Since some of this dust may well originate from disintegrating comets (Vidal–Madjar et al. 1994), this agreement is especially relevant.

The grain size distribution which we postulate for Comets Hale–Bopp and Hyakutake is similar to the β Pic dust. We obtain κ(1 mm)= 75 cm^2 g^{-1}, a factor of 2 higher than the β Pic model. This difference is due to slightly different model assumptions on a_{max} and β. Most importantly, our grain size distribution index $\beta = 3.9$ (Table 8), indicating a larger number of small grains than in the β Pic model ($\beta = 3.5$). Since smaller grains are more efficient (per mass) absorbers, the overall mass absorption cross section is increased in our dust model. In summary, our rudimentary dust model leads us to a mass absorption coefficient at 1 mm wavelength which is at the extreme high end of the range of published κ(1 mm), at variance with the much lower values for normal interstellar dust (e.g. Pollack et al. 1994), but close to model predictions for dust possibly produced in part by disintegrating comets.

By way of comparison, de Pater et al. (1998) and Jewitt & Matthews (1997, 1999) assumed dust opacities appropriate for interstellar dust [κ(1 mm) = 0.5 – 0.55 cm^2 g^{-1}], and derived halo dust masses for Hale–Bopp in the range (3 – 5) 10^{14} g. It is likely, however, that the dust grain population in the cometary

[3] In this paper, the dust absorption cross section κ is always in units of cm^2 per gram of *dust*, not per gram of total mass (dust and gas).

Table 9. Mass and dust production rates, Q, for Hale–Bopp and Hyakutake. For each quantity two values are given, one for "fluffy dust" (κ(1mm) = 75 cm^2/g) and one for "normal interstellar medium" (κ = 0.5 cm^2/g). Dust in comets may have properties bracketted by these extremes (see text).

Comet	Hyakutake		Hale–Bopp	
	fluffy dust	ISM dust	fluffy dust	ISM dust
mass, g	$6 \cdot 10^{10}$	$8 \cdot 10^{12}$	$8 \cdot 10^{12}$	$1 \cdot 10^{15}$
Q, g s^{-1}	$4 \cdot 10^{6}$	$5 \cdot 10^{8}$	$8 \cdot 10^{7}$	$1 \cdot 10^{10}$

halo is quite different from "standard" interstellar dust. The observed spectral index of 2.8 (cf. Fig. 7) suggests that the halo is dominated by large grains, possibly of a "fluffy" or fractal structure. Lisse et al. (1999) find that the IR SED requires a particle size distribution dominated by a mixture of small (1–5 μm) and large ($> 100\,\mu$m) grains, of which the latter would contribute most of the mm and submm flux.

For the Hyakutake halo, Jewitt & Matthews (1997) derive a dust mass of $1.8\,10^{12}$ g from a submm observation within two days from ours. This mass is a factor of 30 higher than our result (Table 8). The difference becomes even larger, a factor of ~ 120, when we take into account the 4 times smaller volume observed by them. This enormous discrepancy is due entirely to different values assumed for κ(1mm). Jewitt & Matthews (1997) adopted a value of κ(1mm) = 0.5 cm^2 g^{-1}, very close to that of normal interstellar dust.

These discrepancies in the derived halo dust masses for both comets reflect to some extent our ignorance of cometary dust properties. We argue that the opacity of cometary dust (at one mm wavelength) may be bracketted by the values for normal interstellar dust, κ_{ISM}, and for the more porous dust, κ_{fd}, described here. Since our models (Sect. 5.2) show that the mm/submm continuum of both comets is clearly optically thin, the derived masses scale inversely with the opacity. The adopted opacitiy range from $\kappa_{ISM} = 0.5$ to $\kappa_{fd} = 75$ cm^{2}g^{-1} therefore implies a mass range by a factor 150. The consequent masses of the particle halos and the dust production rates are assembled in Table 9 for the two comets. We propose that the grain opacities derived for interstellar dust probably underestimate the values appropriate to these comets by at least an order of magnitude, and so lead to corresponding overestimates of the particle halo mass. If the opacity used here, being at the high end of the range of publishes κ(1mm), overestimates the real value of the opacity κ(1mm), the derived halo masses may be too low and so lead to corresponding overestimates of the dust production rate and the dust/gas ratio.

5.8. Discussion of nuclear diameters

In Table 10 the published size determinations are compared with our mean results. The accuracy of the optically-derived sizes is hard to assess, because the values differ even for identical observations. The average value of 48 km may be a good approximation; it agrees well with our estimate derived from the PdB interferometer observations. The quoted lower limits of the VLA observations are derived assuming the equilibrium temperature; if calculated with the sublimation temperature the upper limit on the diameter would be lower by $\sim$20 %). The VLA result by Fernandez, as reported by de Pater et al. (1998), is hard to interpret; the full observing details, the separation of halo and nuclear contribution, the uncertainty of the emissivity at this low frequency are not known yet and may need further discussions. The mean nuclear diameter, derived from the PdBI observations, is quite precise and in agreement with most other determinations of the nuclear size of Comet Hale–Bopp. Unfortunately, this comet was out of reach for radar measurements for an additional confirmation.

For Comet Hyakutake the first size estimate came from radar measurements; the JPL press release from 1996 March 29 reported a size between 1 and 3 km. An improved estimate was given by Harmon et al. (1996). The first reported radio results are given by de Pater et al. (1997) and Fernandez et al. (1997), both assuming the evaporation point of water ice for the brightness temperature. Their limits should be about 20 % higher, if compared to limits based on equilibrium temperatures. Harmon et al. (1997) revised their size estimate, following a re-discussion of the size of Comet IRAS-Araki-Alcock (a secondary calibrator for radar albedo) by Sekanina (1988). This re-discussion leads to bigger sizes of Comet IRAS-Araki-Alcock, which possibly may fit better to the optical data, but which are hard to reconcile with the original radio observations by the VLA and the 100m telescope.

From the radio results of this paper, only the more significant upper limits are included in Table 10. For Comet Hale–Bopp the inner halo contributed to the observed point source; if the same is true for Hyakutake, the radio size of its nucleus might even be below the estimated lower limits. The first estimate of D_n = 2 km by Harmon et al. (1996) may be the better one. Table 10 suggests also that mm-interferometry is best suited for measuring the sizes of cometary nuclei, even though the smallest upper limit in units of Jy is measured at 8.4 GHz (Fernandez et al. 1997).

5.9. Heliocentric distance dependence

In connection with the light curves of the two comets, we considered systematic deviations from the proposed model. In Fig. 10 the integrated and normalized flux densities at 250 GHz are shown as functions of the heliocentric distance. Dots represent data of Comet Hale–Bopp from Pico Veleta, triangles data of Comet Hyakutake from the Heinrich-Hertz-Telescope; the lines are empirical fits to the observations. They confirm qualitatively for radio data, what is known for the optical regime: the activity (brightness) of a comet depends on its heliocentric distance and may be different for each comet. Why do different comets get active and generate a halo at different heliocentric distances? A quantitative confirmation of this result would be helpful for an improved comet model.

Table 10. Derived nuclear diameters

Instrument	ν [GHz]	Date	D_n [km]	Reference
a.) Comet Hale–Bopp				
HST	opt.	Oct. 95	27. - 42.	Weaver et al. (1997)
HST	opt.	Oct95-Sept96	73.	Sekanina (1998)
HST	opt.	Oct. 96	$\sim$50.	Sekanina (1998)
PdB IF	90 & 220	Mar. 97	44.2	this paper
VLA	22.5	Apr. 97	$\leq$ 93.	de Pater et al. (1998)
VLA	43.	Apr. 97	$\leq$ 45.	de Pater et al. (1998)
b.) Comet Hyakutake				
Goldstone	8.51	Mar 24/5,96	$\sim$2.0	RADAR, Harmon et al. (1996)
BIMA array	111.5	Mar 24/6,96	$\leq$ 5.0	de Pater et al. (1997)
VLA	8.45	Mar 27,1996	$\leq$ 6.0	Fernandez et al. (1997)
Goldstone	8.51	Mar 24/5,96	$\sim$2.5	RADAR. Harmon et al. (1997)
VLA	22.5	Mar 25,1996	$\leq$ 4.2	this paper
PdB IF	88.6	Mar 23,1996	$\leq$ 3.3	this paper
PdB IF	241.3	Mar 24,1996	$\leq$ 2.1	this paper

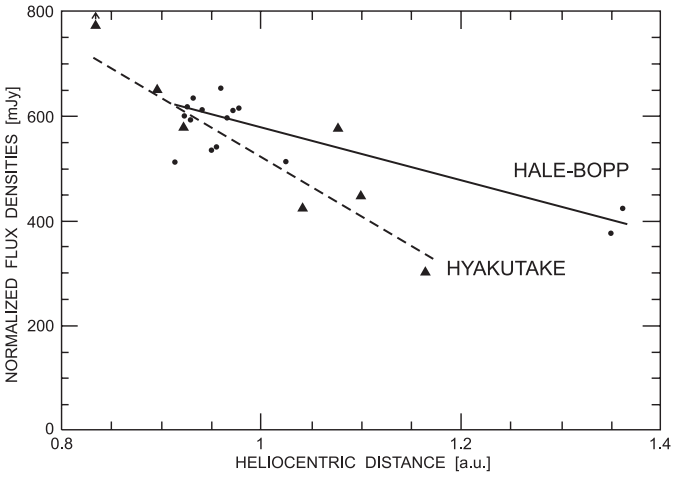

Fig. 10. The normalized flux density of Comets Hale–Bopp and Hyakutake as function of heliocentric distance

Table 11. Comparison of cometary parameters

Comet	Halley	Hyakutake	Hale–Bopp
Nucleus			
geom. Albedo	0.03	0.03	0.03
mean diameter [km]	10.	2.	44.2
mass [g]	$5{\cdot}10^{17}$	$4{\cdot}10^{15}$	$5{\cdot}10^{19}$
rot. period [h]	52.	6.25?	11.47
Halo			
gauss diam. [km]	3800.	1870.	11080.
mass* [g]	$2{\cdot}10^{13}$	$6{\cdot}10^{10}$	$8{\cdot}10^{12}$
ph. diam.(250) [km]	35.	17.1	233.
Spectral Index α	2.3$\pm$0.4	2.8$\pm$0.1	2.8$\pm$0.1
dust p. rate Q* [g s^{-1}]	$2.9{\cdot}10^{6}$	$4{\cdot}10^{6}$	$8{\cdot}10^{7}$

* based on κ_{fd} (Table 9)

5.10. Comparison of the three best observed radio comets

Table 11 summarizes the physical properties of Comets Halley, Hyakutake and Hale–Bopp (which are the best-observed comets at radio frequencies). The size of Comet Halley was taken from the *Giotto* measurements; the other two are from this paper. The mass is calculated from the mean geometric size by assuming a density of 1 g cm^{-3}; the rotation periods are from literature. The data on the halo of Comet Halley are from Altenhoff et al. (1989), except for the mass loss rate, which was taken from McDonnell et al. (1987); the other values are from this paper. The photometric diameter is an observational parameter; it seems to correlate linearily with the nuclear size. The SED of Comet Halley is ill defined because of the small frequency basis and the limited accuracy of the heterodyne receiver data. In hindsight we would not be surprised if the spectral index α of Comet Halley were similar to that of the other comets, i.e. showing a similar particle mix, which is also supported by the particle mix seen by *Giotto* (McDonnell et al. 1987). The halo mass estimate for Comet Halley was derived by a higher size cutoff as for the other comets, thus giving higher masses. The dust production rate of Comet Halley with an upper particle cutoff of 1 g was taken from McDonnell et al. (1987); with an extrapolated cut off of 1 kg the dust production rate would become a factor of 7 higher, equalizing dust and gas production rates for Comet Halley.

6. Summary

The continuum radiation of these comets can be described by the point source like emission of the nucleus and the extended halo emission, originating by the r^{-2} density distribution being in thermal equilibrium with insolation. The center of the halo coincides with the nucleus. The inner part of the halo seems to be circularly symmetric. The steady "light" curve of the comets can

be described by its geo- and heliocentric distances. The observed inner halo can be approximated by a Gaussian; the extended structure neglected in the Gaussian approximation contains 30 to 40 % of the flux density, depending on integration limits. The brightness temperature of the nucleus is probably close to equilibrium temperature and allows a determination of its size. The three most intensively observed "radio" comets seem to have a similar power law spectrum, indicating a similar particle spectrum. The apparent correlation of photometric diameter, halo size and mass, and dust production rate on the one hand and the nuclear mass on the other needs further proof. During the monitoring time none of these comets showed any significant internal variability or any transient outburst or IGH event.

Acknowledgements. We greatly appreciate the support by Dr. H. Ungerechts, IRAM Granada, and by D. Ashby and J. Glenn, Steward Observatory, who carried out some of these observations. We acknowledge the help of Dr. P. Rocher of the Bureau des Longitude, Paris for preparing the ephemerides for the PdBI, using the latest sets of orbital elements of Dr. D.K. Yeomans of JPL, Pasadena. We acknowledge helpful advice by Dr. E. Krügel, Bonn, and we are very grateful to Dr. D. Bockelée-Morvan, Paris, for providing molecular line frequencies for editing the continuum data and we thank her and her colleagues for the efficient collaboration at the Plateau de Bure during the shared line and continuum observations. JHB thanks Dr. Casey Lisse for helpful discussion.

References

Aguirre E.L., 1997, S&T 93 5, 28
Altenhoff W.J., Batrla W., Huchtmeier W.K., et al., 1983, A&A 125, L19
Altenhoff W.J., Huchtmeier W.K., Kreysa E., et al., 1989, A&A 222, 323
Altenhoff W.J., Johnston K.J., Stumpff P., Webster W.J., 1994, A&A 287, 641
Altenhoff W.J., Bieging J.H., Butler B., et al., 1996, BAAS 28, 928
Bieging J.H., Mauersberger R., Altenhoff W.J., et al., 1997, BAAS 29, 1319
Biver N., Bockelée-Morvan D., Colom P., et al., 1997, Sci 275, 1915
Broguiere D., Neri R., Sievers A., et al., 1996, NIC, IRAM manual version 1.0
Crifo J.F., 1987, Improvements in hydrodynamic models of Comet Halley dusty atmosphere: initial boundary conditions and homogeneous nucleation. In: Battrick B., Rolfe E.J., Reinhard R. (eds.) 2nd ESLAB symposium on the exploration of Halley's comet. ESA SP-250 I, 533
Crovisier J., Schloerb F.P., 1991, The Study of Comets at Radio Wavelengths. In: Newburn R.L., Neugebauer M., Rahe J. (eds.) Comets in the Post-Halley Era. Kluwer, Dordrecht, p. 149
de Pater I., Wade C.M., Houpis L.L.F., Palmer P., 1985, Icarus 62, 349
de Pater I., Snyder L.E., Mehringer D.M., et al., 1997, Planet. Space Sci. 45, 731
de Pater I., Forster J.R., Wright M., et al., 1998, AJ 116, 987
Draine B.T., Lee H.M., 1984, ApJ 285, 89
Fanale F.P., Salvail J.R., 1984, Icarus 60, 476
Fernandez Y.R., Kundu A., Lisse C.M., A'Hearn M.F., 1997, Planet. Space Sci. 45, 735
Garcia-Burillo S., Guelin M., Cernicharo J., 1993, A&A 274, 123
Gregory P.C., Condon J.J., 1991, NRAO preprint 90/91
Guilloteau S., Lucas R., Bouyoucef K., 1997, GRAPHIC/MAPPING IRAM manual version 1.2
Hanner M.S., Aitken D.K., Knacke R., et al., 1985, Icarus 62, 97
Harmon J.K., Ostro S.J., Roesema K.D., et al., 1996, BAAS 28, 1195
Harmon J.K., Ostro S.J., Benner L.A.M., et al., 1997, Sci 278, 1921
Hellyer B., 1970, MNRAS 148, 383
Hobbs R.W., Maran S.T., Brandt J.C., et al., 1975, ApJ 201, 749
Jewitt D.C., Luu J., 1992, Icarus 100, 187
Jewitt D.C., Matthews H.E., 1997, AJ 113, 1145
Jewitt D.C., Matthews H.E., 1999, AJ 117, 1056
Kammerer A., 1997, Schweifstern 13, Heft 71,3
Krishna-Swany K.S., 1986, Physics of Comets. World Sci. Publ., Singapore
Kreysa E., Altenhoff W.J., Haslam C.G.T, Sievers A., 1997, IAU Circular 6555
Krügel E., Siebenmorgen R., 1994, A&A 288, 929
Lecacheux J., Jorda L., Colas F., 1997, IAU Circ. 6560
Lisse C.M., Fernandez Y.R., A'Hearn M.F., et al., 1999, Earth, Moon, and Planets. In press
Lucas R., 1996, CLIC, IRAM manual 4.1
Marsden B.G., 1996, Minor Planet Circular #28557
Marsden B.G., 1997, Minor Planet Circular #29067
Mathis J.S., Rumpl W., Nordsieck K.H., 1977, ApJ 217, 425
Matthews H.E., Holland W., Meier R., Jewitt D.C., 1997, IAU Circular 6609
McDonnell J.A.M., Alexander W.M., Burton W.M., et al., 1987, A&A 187, 719
Menshchikov A.B., Henning T., 1996, A&A 318, 879
Ott M., Witzel A., Quirrenbach A., et al., 1994, A&A 284, 331
Pollack J.B., Hollenbach D., Beckwith S., et al., 1994, ApJ 421, 615
Sandell G., 1994, MNRAS 271, 75
Sekanina Z., 1988, AJ 95, 1876
Sekanina Z., 1998, JPL Cometary Sci. Team preprint No. 172, also Earth, Moon, and Planets. In press
Vidal-Madja A., Lagrange-Henri A-M., Feldman P.D., et al., 1994, A&A 290, 245
Walmsley C.M., 1985, ApJ 297, 677
Weaver H.A., Feldman P.D., A'Hearn M.F., et al., 1997, Sci 275, 1900
Wink J.E., Bockelée-Morvan D., 1997, IAU Circular 6587
Wink J.E., Thum C., Altenhoff W.J., et al., 1999, Earth, Moon, and Planets. In press
Yeomans D.K., 1991, Comets. Wiley Science Editions, New York, p. 292
Zylka R., 1997, MOPSI, mapping software, ITA, Heidelberg